Anais da Academia Brasileira de Ciências
ISSN: 0001-3765
aabc@abc.org.br
Academia Brasileira de Ciências
Brasil

de Almeida, Delia Del Pilar M.; Pereira, Vitor P.; Machado, Adriane; Zerfass, Henrique; Freitas, Ricardo

Late sodic metasomatism evidences in bimodal volcanic rocks of the Acampamento Velho Alloformation, Neoproterozoic III, southern Brazil

Anais da Academia Brasileira de Ciências, vol. 79, núm. 4, 2007, pp. 725-737
Academia Brasileira de Ciências
Rio de Janeiro, Brasil

Anais da Academia Brasileira de Ciências (2007) 79(4): 725-737
(Annals of the Brazilian Academy of Sciences)
ISSN 0001-3765
www.scielo.br/aabc

Late sodic metasomatism evidences in bimodal volcanic rocks of the Acampamento Velho Alloformation, Neoproterozoic III, southern Brazil

DELIA DEL PILAR M. DE ALMEIDA[1], VITOR P. PEREIRA[2], ADRIANE MACHADO[3], HENRIQUE ZERFASS[4] and RICARDO FREITAS[5]

[1]PPGeo, Universidade do Vale do Rio dos Sinos (UNISINOS), Av. Unisinos, 950, Cristo Rei
93022-000 São Leopoldo, RS, Brasil
[2]Instituto de Geociências, Universidade Federal do Rio Grande do Sul (UFRGS), Caixa Postal 15001
91509-900 Porto Alegre, RS, Brasil
[3]Centre for Geophysics of the University of Coimbra-CGUC, Av. Dr. Dias da Silva, 3000-134 Coimbra, Portugal
[4]Companhia de Pesquisa de Recursos Minerais, rua Banco da Província, 105, 90849-030 Porto Alegre, RS, Brasil
[5]UNISINOS, Av. Unisinos, 950 Cristo Rei, 93022-000 São Leopoldo, RS, Brasil

Manuscript received on April 9, 2006; accepted for publication on March 28, 2007;
presented by LEO A. HARTMANN

ABSTRACT

A mineralogical study was carried out in mafic and felsic volcanic rocks of the Acampamento Velho Alloformation at Cerro do Bugio, Perau and Serra de Santa Bárbara areas (Camaquã Basin) in southern Brazil. The Acampamento Velho bimodal event consists of two associations: lower mafic at the base and upper felsic at the top. Plagioclase and alkali-feldspar were studied using an electronic microprobe, and magnetite, ilmenite, rutile, illite and alkali-feldspar were investigated through scanning electron microscopy. The rocks were affected by a process of late sodic autometasomatism. In mafic rocks, Ca-plagioclase was transformed to albite and pyroxenes were altered. In felsic rocks, sanidine was partially pseudomorphosed, generating heterogeneous alkali-feldspar. In this association, unstable Ti-rich magnetite was replaced by rutile and ilmenite. In mafic rocks, the crystallization sequence was: (1) Ti-rich magnetite (?), (2) pyroxene and Ca-plagioclase, (3) albite (alteration to Ca-plagioclase), (4) sericite, chlorite and calcite (alteration to pyroxene), and kaolinite (alteration to plagioclase/albite). In felsic rocks: (1) zircon, (2) Ti-rich magnetite, (3) sanidine, (4) quartz. The introduction of late Na-rich fluids, generated the formation of (5) heterogeneous alkali-feldspar, (6) ilmenite and rutile from the Ti-rich magnetite, (7) albite in the spherulites. Finally, alteration of sanidine, vitroclasts and pumice to (8) illite.

Key words: chemical mineral, sodic metasomatism, Acampamento Velho Alloformation, Brazilian Orogeny.

INTRODUCTION

The Camaquã Basin developed during the final stages of the Brazilian-Pan-African Orogeny (700 m.y–540 m.y.) in the Sul-rio-grandense Shield. This basin formed in a retroarc-foreland setting and was filled essentially by clastic sediments. During some stages of basin evolution, volcanism was intense and resulting in the emplacement of felsic and intermediate volcanic rocks genetically associated with granites. The origin and evolution of the Camaquã Basin has been hardly discussed over the last 15 years. The main hypotheses for the formation of the Camaquã Basin include strike-slip Fernandes (1992), late to post-tectonic foreland (Gresse et al. 1996, Basei et al. 2000), retroarc (Chemale Jr. 2000) and intraplate basin (Fragoso-Cesar et al. 2000).

During the late stages of Brazilian / Pan-African Orogeny (Neoproterozoic III), the Camaquã Basin was gradually filled by the bimodal volcanic rocks of alka-

Correspondence to: Delia del Pilar M. de Almeida
E-mail: lesda@terra.com.br

line composition of the Acampamento Velho Alloformation (AVAf) (Paim et al. 2000). It has been traditionally considered as exclusively acid in composition, but detailed geological mapping at the Cerro do Bugio, Cerro do Perau and Santa Bárbara area (west of Caçapava do Sul town) revealed the existence of a basalts/andesite unit at the base and a felsic unit at the top (Zerfass and Almeida 1997, Zerfass et al. 2000, Almeida et al. 2002), that leads to the existence of a bimodal alkaline volcanism: mafic at the base and a felsic unit at the top. Sommer et al. (1999) described the existence of a sequence of effusive, pyroclastic and volcanic comenditic rocks at the Taquarembó Plateau. In the same area, Wildner et al. (1999) verified that these rocks are alkaline, satured in silica, and have post-collisional characteristics. Sommer et al. (2005) recognized the existence of a bimodal mildly alkaline magmatism related to post-collisional events at the Ramada Plateau.

The detailed mineralogic study of this volcanic sequence through scanning electron microscopy (SEM) and electron microprobe (EMP) is important to improve the understanding of the petrologic evolution of the rocks in this sequence and consequently this important volcanic episode.

GEOLOGICAL SETTING

The area is a long, narrow N20°E ridge formed by the AVAf volcanic rocks, where the main elevations are Cerro do Bugio (419 m), Cerro do Perau (331 m) and Serra de Santa Bárbara (440 m), from north to south (Fig. 1). In this area, an unconformity marks the lower contact of the AVAf over the sedimentary rocks of the Maricá or Bom Jardim allogroups (sensu Paim et al. 2000). The upper contact of the AVAf with the Santa Fé or Lanceiros alloformations (sensu Paim et al. 2000) is delineated by a disconformity. The AVAf is composed of a Lower Mafic Association (LMA) and an Upper Felsic Association (UFA).

The Lower Mafic Association is composed by basalts and andesitic basalts flows (BasA-A), as well as subordinate andesitic breccias that occur as a continuous bed, with thickness between 10 m and 350 m. It is usually massive, with rare stratification, dipping about 20° to the E or SE. This rocks show porphyritic texture with plagioclase phenocrysts (Almeida et al. 2002).

The Upper Felsic Association is composed of rhyolitic rocks. The rhyolitic association comprises alternating pyroclastic rocks (lapilli-tuffs, tuffs, welded tuffs) and flows at the top. Its stratification is tilted, dipping about 20° to the E or SE. The lapilli-tuffs are preserved as discontinuous strata of thicknesses up to 40 m. The tuffs occur as lenses of variable thickness (up to 30 m) and internally consist of parallel layers, poorly sorted in general terms. The welded tuffs are also poorly sorted, and they present predominantly ash fraction and occur as lenticular layers up to 350 m thick. The rhyolitic flows form a continuous layer of variable thickness from 20 m to 600 m. Internally, they display flow foliation, which is frequently folded (Zerfass and Almeida 1997).

The lapilli-tuffs, tuffs and welded tuffs are interfingered and associated with pyroclastic flows generated during the rhyolitic eruptive phase, as a product of the eruptive column collapse. Pyroclastic fall processes are predominant in distal regions, as it is suggested by the well sorting of the finer tuff members. The rhyolitic flows overlie all of the previous facies, suggesting that the Upper Felsic Association is related to plinian volcanism (Zerfass et al. 2000).

The first geochronological investigation in the AVAf rhyolites was performed by Cordani et al. (1974), followed by Sartori (P.L.P. Sartori, unpublished data) and Teixeira (1982). Soliani Jr. (E. Soliani Jr., unpublished data) compiled their data and obtained an age of 529 ± 4 m.y. (Rb-Sr, whole rock reference isochron considering $R_0 = 0.7057$). Another Rb-Sr dating was performed by Almeida et al. (2002), who studied the rhyolitic flows of Cerro do Bugio area and the dykes intruding the Maricá Formation. These authors obtained two whole rock isochrons: 545.1 ± 12.7 m.y. ($R_0 = 0.70932$) and 546 ± 12.9 m.y. ($R_0 = 0.71454$) (Almeida et al. 2002). Chemale Jr. (2000) obtained an U/Pb zircon age of 573 ± 18 m.y., εNd ($t = 570$ m.y.) of –9.34 and –9.37, and T_{DM} model ages from 1.7 to 1.9 Ga. Sommer et al. (2005) used SHRIMP U/Pb dating in eleven zircon crystals from rhyolites of the AVAf at the Vila Nova do Sul area, and presented an age of 549.3 ± 5 m.y. Therefore, all the ages obtained so far indicate that this alloformation belongs to the Late Neoproterozoic III.

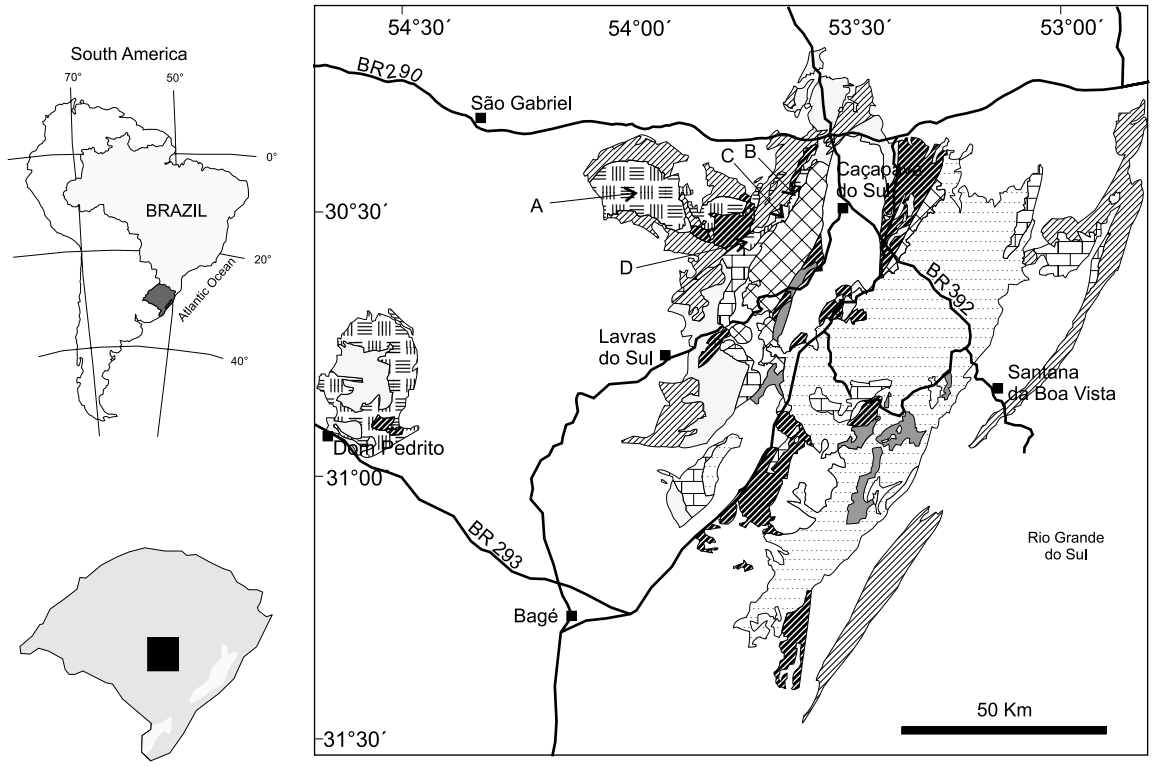

Fig. 1 – Simplified geologic map of the Camaquã Basin (after Paim et al. 2000) showing the studied localities.

TECTONIC CONTEXT AND GEOCHEMICAL CHARACTERIZATION

Almeida et al. (2005) consider that the isotopic signature of AVAf (lower mafic association) is a mixture of depleted mantle-derived basalts with 20% to 30% of crustal contamination by sediment (probably Neoproterozoic arkosic quartzites). The formation of a magmatic chamber and the separation of the magma into two fractions gave rise initially to the mafic rocks at the base of the Acampamento Velho Alloformation. The other magma fraction gave place to a significant enrichment in crustal components before the felsic pyroclastic rocks and before flows formed at the top (upper felsic association).

According to Almeida et al. (2002, 2003), the AVAf have been generated in an extensional regime preceding the collision of the Rio de la Plata and the Kalahari con-

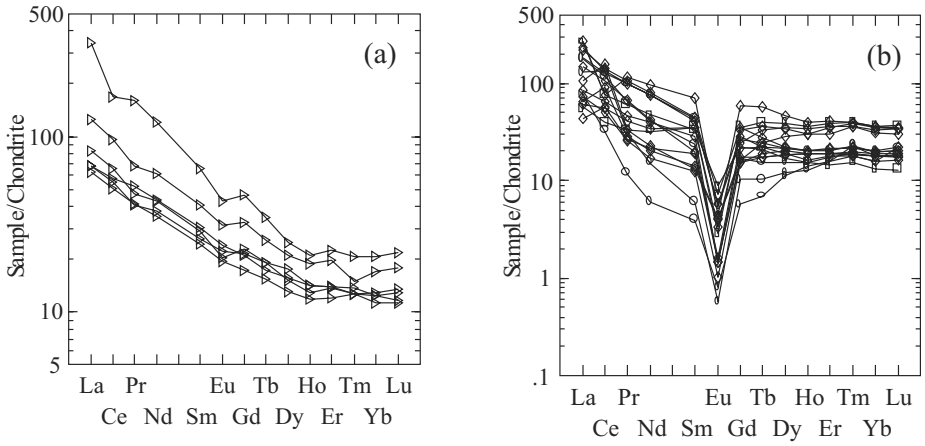

Fig. 2 – Chondrite Normalized (Taylor and MacLennan 1985) REE diagram for the (a) Lower Mafic Association and (b) Upper Felsic Association: □ = tuffs, o = welded tuffs, ◊ = flows (after Almeida et al. 2002).

tinental plates. Therefore it is a magmatism generated in a continental arc. According to Chemale Jr. (2000), the Nama Basin (in the African counterpart) was generated during the collisional phase, and it is a foreland peripheral basin associated with transcurrent reactivations. This author also suggests that in Rio Grande do Sul the sin-, tardi- and post-transcurrent granites, from Erval, Viamão, Encruzilhada do Sul, Cordilheira and Dom Feliciano suites, are associated with this collisional phase. This extensional regime probably occurred during the final phases of subduction of the Adamastor Oceanic plate beneath the continental Rio de la Plata plate in a retroarc setting. This subduction took place between 650 m.y and 540 m.y. (Chemale Jr. 2000), just before the collision of the Kalahari and the Rio de la Plata continental plates.

The following data is a summary of the geochemical behavior of rocks from AVAf, reported by Almeida et al. (2002, 2003).

In the LMA group, whole-rock analyses showed an average SiO_2 content of 49.48%; Na_20 = 4.30%, K_20 = 0.85% and CaO = 3.06%.

The behavior of REE pointed out to a moderate alkaline character of the LMA (Fig. 2a), with high La/Yb_N ratios ($5.30 < La/Yb_N < 7.38$, average of 6.16), and Eu/Sm_N ratios ($0.69 < Eu/Sm_N < 0.81$, average of 0.76). The LREE patterns show relatively low fractionation ($2.24 < La/Sm_N < 3.07$, average of 2.72), with a very slight Eu negative anomaly ($0.95 < Eu_N/Eu^* < 0.79$, average of 0.89) (Fig. 2a).

In the UFA, the tuff samples have a SiO_2 average of 73.09%, with a low alkalinity (average of Na_20 = 1.53% and K_20 = 3.96%), and high CaO content (2.98%). The LREE pattern shows slight fractionation ($1.65 < La/Sm_N < 7.92$, average of 4.71), with a variable Eu negative anomaly (Eu_N/Eu^* = 0.08 to 0.32, average of 0.18).

The welded tuffs are also highly siliceous, with SiO_2 average of 78.20%, low CaO (average of 0.06%), and the alkalinity higher than tuffs (average of Na_2O = 1.71% and K_2O = 5.75%). The REE behavior is similar to the tuffs, although they present much more pronounced fractionation of LREE ($4.1 < La/Sm_N < 21.2$, average of 7.27), and an important Eu negative anomaly ($0.07 < Eu_N/Eu^* < 0.16$, average of 0.12).

Likewise, the rhyolitic flow samples are also siliceous, with SiO_2 average of 77.2%, low CaO (average of 0.17%) and normal alkalinity, although these rocks are more sodic than the pyroclastic ones (average of Na_2O = 2.12% and K_2O = 5.34). The REE pattern is similar to those of tuffs and welded tuffs, with fractionation of the LREE ($1.73 < La/Sm_N < 12.16$, average of 4.55) and Eu negative anomaly ($0.06 < Eu_N/Eu^* < 0.28$, average 0.12).

The LREE fractionation in the rhyolitic flows is slighter than that observed during the passage from tuffs to welded tuffs, and the Eu anomaly is similar to that of the welded tuffs. The REE diagram of UFA (Fig. 2b)

exhibits values corresponding to the evolved rocks, similar to those of Cullers and Graf (1984), showing moderate fractionation and clear parallelism, especially of HREEs and confirming the alkaline character. The increasing values of REE and a marked negative Eu anomaly are common in the felsic rocks (UFA) associated with mafic one (LMA).

The data presented above suggest that the evolution of magmatism from the LMA to the UFA associations took place with an increase in SiO_2, MgO, FeOt, Na_2O and K_2O, and a pronounced decrease in CaO. This is particularly marked at the transition from tuffs to welded tuffs. In addition, the LREE fractionation and the important increase of the Eu negative anomaly are observed. The passage from welded tuffs to rhyolitic flows is marked by a change in the behavior of the alkalis, with an increase in Na_2O and CaO, and decrease in K_2O.

According to Almeida et al. (2002, 2003), the bimodal volcanism of the AVAf is characterized by the presence of dominant acid and subordinated mafic rocks, with overall absence of rocks with SiO_2 content between 54% and 67%. The Nb $\times$ Zr and Y $\times$ Zr ratios show different evolutionary trends for the mafic and felsic successions, reinforcing the bimodal character of this magmatism. The behavior of REE, some trace elements and isotopic signature (Sm/Nd, Rb/Sr) suggest a common magmatic source for the LMA and UFA associations.

ANALYTICAL METHODS

The mineral chemistry analyses were performed by scanning electron microscopy (SEM) and electron microprobe (EMP) at the Federal University of Rio Grande do Sul (UFRGS). SEM was used to study heterogeneous feldspar, magnetite, ilmenite, rutile, shards, fiammes and pumice structures. EMP was used to analyze plagioclase, alkali feldspar, quartz and spherulites.

Mineral compositions were determined by Wavelength Dispersive Spectroscopy (WDS) using a CAMECA SX-50. Analyses were performed at 15 KeV and 10 nA. The spot size was 1 μm and the counting time was 20s. Full ZAF corrections were applied to the raw X-ray data. The following standards were employed for the determination of mineral composition:

TAP:$^{-1}$FKα(CaF_2), ^{1}NaKα (JADE), ^{4}SiKα (ANOR), ^{5}TaMα (Ta);

LIF:^{2}FeKα (MnOH), ^{3}LaLα (Ree3);

PET:^{1}K Kα (ASBE), ^{2}Ca Kα (ANOR), ^{4}Ti Kα (TiO_2), ^{3}Ce Lα (Ree3), ^{4}U Mα (xGLA).

Back-scattered electron (BSE) images were acquired using a JEOL, JSM-5800 and performed at 20 Kv, and 25 nA for or during 100s.

MINERAL CHEMISTRY

In the LMA, the basalts and andesitic basalts (BasA-A) show relict pilotaxitic texture and zoned plagioclase phenocrysts with diffuse appearance. Sericite, kaolinite, carbonate, chlorite and opaque minerals replace totally the pyroxene phenocrysts and sometimes, partially the plagioclase. Quartz, plagioclase and sanidine grains present on the top layers incipient "kidney-shaped" texture. The matrix is formed by plagioclase microliths, chlorite-carbonate, a ferro-magnesian pseudomorph (pyroxene?) and a large quantity of opaque minerals (Almeida et al. 2002). EMP analyses show that plagioclase phenocrysts and matrix are sometimes totally albitized, with compositions between $Ab_{99.6}$ and Ab_{98} (Fig. 3).

The lapilli-tuffs of UFA contain poorly sorted lithoclasts (3 to 40 mm in diameter), vitroclast pseudomorphs (cuspate and platy shapes) substituted by silica and phyllosilicates, quartz crystalloclasts with corrosion gulfs, sanidine and heterogeneous alkali-feldspar. The latter is produced by the sodic metassomatic alteration of sanidine, forming heterogeneous pseudomorphs where part of sanidine is transformed to albite. The matrix of lapilli-tuffs is tuffaceous and microcrystalline. The tuffs and welded tuffs differ from each other on the degree of welding. They contain crystalloclasts of euhedral quartz or with corrosion gulfs, heterogeneous alkali-feldspar, sanidine (altered to phyllosilicates) and magnetite. The tuffaceous matrix is composed of cuspate and platy-shaped fragments (pseudomorphs of volcanic glass shards) and pumice shard-shaped fragments in the welded tuffs, suggesting pumice pseudomorphs. Eutaxitic flow structures, conchoidal fractures and perlitic textures are common (Fig. 4a). Original glass is strongly devitrified. Spherical spherulitic and axiolitic spherulites structures occur subordinately.

	phenocrysts			matrix		matrix		phenocrysts			matrix
Sample	MH13-10	MH13-12	MH13-13	MH13-14	MH13-15	MH13-16a	MH13-16b	MH13-1a	MH13-6a	MH13-6b	MH13-8
Location	rim	core	core	core	rim	core	rim	core	core	rim	core
SiO_2	71.05	71.65	70.52	71.24	71.23	70.42	71.60	71.37	71.20	70.77	71.51
Al_2O_3	19.97	19.65	20.20	19.84	19.96	20.08	20.18	19.88	20.22	20.38	19.74
FeO	0.35	0.09	0.12	0.05	0.03	0.14	0.22	0.04	0.58	0.21	0.31
MgO	0.03	n.d.	n.d.	n.d.	n.d.	0.01	0.04	0.01	0.10	0.01	n.d.
BaO	0.06	0.08	0.07	n.d.	n.d.	n.d.	0.01	0.07	n.d.	0.03	0.17
CaO	0.13	0.04	0.08	0.09	0.07	0.03	0.06	0.04	0.05	0.25	0.07
Na_2O	10.25	10.34	10.43	10.45	10.09	9.99	10.35	10.64	10.40	9.89	10.14
K_2O	0.10	0.02	0.17	0.03	0.05	0.09	0.02	0.04	0.09	0.11	0.13
Total	101.94	101.87	101.59	101.70	101.43	100.76	102.48	102.09	102.64	101.65	102.07
Si	6.05	6.50	6.03	6.47	6.07	6.05	6.05	6.47	6.03	6.03	6.50
Al	2.00	2.10	2.03	2.12	2.00	2.03	2.01	2.12	2.02	2.05	2.11
Fe_2	0.02	0.01	0.01	n.d.	n.d.	0.01	0.02	0.01	0.04	0.02	0.02
Mg	n.d.	n.d.	n.d.	n.d.	n.d.	n.d.	0.01	n.d.	0.01	n.d.	n.d.
Ba	n.d.	n.d.	n.d.	n.d.	n.d.	n.d.	n.d.	n.d.	n.d.	n.d.	0.01
Ca	0.01	n.d.	0.01	0.01	0.01	n.d.	0.01	n.d.	0.01	0.02	0.01
Na	1.69	1.82	1.73	1.84	1.67	1.66	1.70	1.87	1.71	1.64	1.78
K	0.01	n.d.	0.02	n.d.	0.01	0.01	n.d.	n.d.	0.01	0.01	0.02
Cations	9.80	10.43	9.83	10.45	9.76	9.77	9.79	10.47	9.82	9.77	10.43
X	8.05	8.59	8.06	8.59	8.08	8.08	8.06	8.59	8.05	8.08	8.59
Z	1.75	1.83	1.77	1.86	1.68	1.69	1.72	1.89	1.77	1.69	1.83
Ab	98.70	99.60	98.50	99.30	99.20	99.20	99.50	99.60	99.20	98.00	98.70
An	0.70	0.20	0.40	0.50	0.40	0.20	0.40	0.20	0.20	1.30	0.40
Or	0.64	0.16	1.08	0.22	0.36	0.60	0.12	0.21	0.58	0.72	0.89

Fig. 3 – Table of analyses of albitized plagioclase (electron microprobe) from basalt and andesitic basalt flows of Lower Mafic Association – Acampamento Velho Alloformation. n.d. = not detected.

Tuff analyses by EMP (Table I) show that the alkali-feldspar crystalloclasts are totally albitized ($Ab_{99.6}$ to $Ab_{98.9}$). SEM analyses show that alkali-feldspar is also heterogeneous, and contain albite and sanidine in the same crystals. Albite is the product of sanidine alteration. These tuffs display shard pseudomorphs devitrified to illite (Fig. 4b), and crystalloclasts of sanidine with illite pseudomorphs (Fig. 4c). Magnetite is Ti-rich (Table II) and has inclusions of zircon grains, which are also located around the grain edges. Ti- rich magnetite is pseudomorphically replaced by sanidine and ilmenite (Table II) along cleavages planes, and their edges are partially corroded by reaction with the matrix (Fig. 4d).

The analyses of welded tuffs by EMP (Fig. 5) show that the alkali-feldspar crystalloclasts are composed predominantly by sanidine with variable amounts of albite and K-sanidine (Fig. 6a). The matrix contains predominantly K-sanidine and but also sanidine Na-rich (Ab = 32.4). Plagioclase crystalloclasts (andesine-labradorite) are present in some samples. The welded tuffs present pseudomorph pumices in fiammes, heterogeneous alkali-feldspar and sanidine crystalloclasts that are altered to illite and sometimes corroded by matrix (Fig. 6b). The Ti-rich magnetite crystalloclasts are altered to ilmenite and rutile (Table II), which are disposed according to twinning and/or cleavage planes (Fig. 6c), and sometimes replaced by sanidine. Homogeneous and zoned zircons usually occur as inclusions, similar to those observed in tuffs, in heterogeneous alkali-feldspar and quartz. The matrix of welded tuffs consists of sanidine and quartz stretched as pseudomorphic shards and pumice, suggesting a strong devitrification of these rocks (Fig. 6d).

The rhyolitic flows are homogeneous or banded. Relict structures of perlitic devitrification and conchoidal fractures are common in the microfelsitic matrix. Sanidine, heterogeneous alkali-feldspar and quartz phenocrysts display corrosion gulfs and conchoidal fractures (Fig. 7a). Iron oxide/hydroxide and sericite are also present as alteration products. Rhyolitic flows, when banded, show an intercalation of thick spherical spherulites, product of devitrification, and microcrystalline bands of quartz and feldspar. EMP analyses of spherulites show that they have heterogeneous composition, with fine aggregates of anorthoclase and albite grains

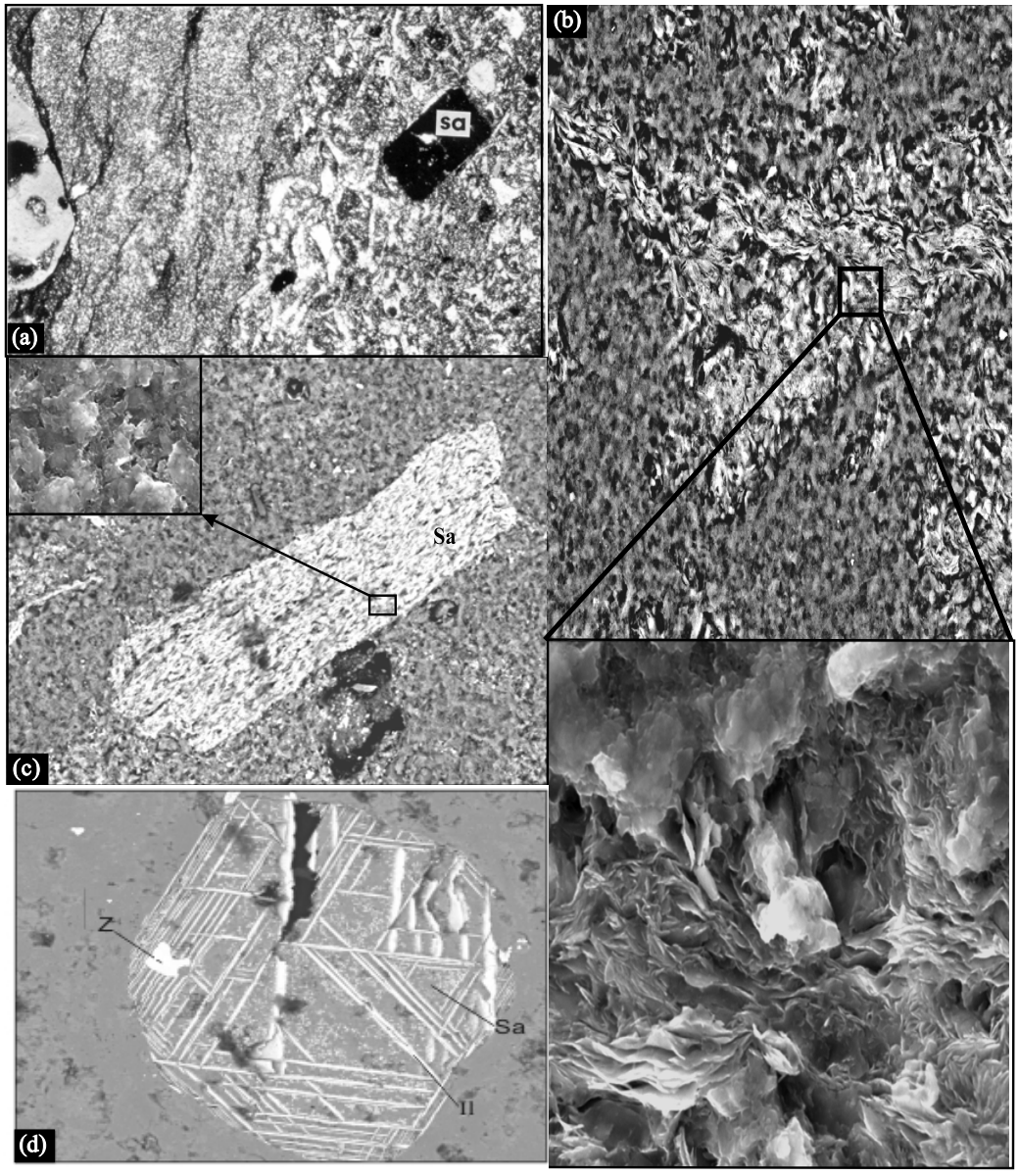

Fig. 4 – Tuff: (a) Photomicrography of cuspate and platy-shaped fragment, pseudomorphs of volcanic shards; pumice and fiammes (optical microscope PL); (b) Photomicrography of glass shard with pseudomorphic substitution by illite (SEM); (c) Photomicrography of crystalloclast of sanidine altered to illite (SEM); (d) Photomicrography of crystalloclast of Ti-rich magnetite pseudomorphically replaced by ilmenita and sanidine with inclusions of zircon (SEM).

(Fig. 7b). Analyses of rhyolitic flows by EMP (Fig. 8) show that the alkali-feldspar phenocrysts consist of sanidine, albite and heterogeneous alkali-feldspar (Figs. 7c and 7d). SEM analyses indicate that Ti-rich magnetite (Table II) and zircon are similar to those described before.

CONCLUSIONS – LATE SODIC METASOMATISM

The basalts and andesitic basalts of LMA show zoned pyroxene and plagioclase phenocrysts. The matrix consists of plagioclase and pyroxene(?) microliths and opaque

TABLE I
Analyses of albite (EMP) from rhyolitic tuffs of Upper felsic Association – Acampamento Velho Alloformation. n.d. = not detected.

Sample	MH161a	MH161b	MH163a	MH 163b	MH165a	MH165b
Location	core	rim	core	rim	core	rim
SiO_2	71.10	71.80	70.85	71.63	71.06	71.06
Al_2O_3	19.96	20.13	20.10	20.07	20.12	20.12
FeO	0.05	n.d.	0.04	n.d.	n.d.	n.d.
BaO	0.10	0.01	n.d.	0.10	0.04	0.04
CaO	0.14	0.05	0.02	0.04	0.04	0.04
Na_2O	10.07	9.96	10.20	10.40	10.63	10.63
K_2O	0.06	0.11	0.03	0.06	0.04	0.04
Total	101.48	102.06	101.24	102.31	101.94	101.94
Si	6.066	6.08	6.05	6.06	6.04	6.04
Al	2.01	2.01	2.02	2.00	2.01	2.01
Fe_2	n.d.	n.d.	n.d.	n.d.	n.d.	n.d.
Ba	n.d.	n.d.	n.d.	n.d.	n.d.	n.d.
Ca	0.01	n.d.	n.d.	n.d.	n.d.	n.d.
Na	1.17	1.64	1.69	1.71	1.75	1.75
K	0.01	0.01	n.d.	0.01	0.01	0.01
Cations	9.77	9.74	9.78	9.79	9.82	9.82
X	8.07	8.09	8.08	8.07	8.06	8.06
Z	1.69	1.65	1.70	1.72	1.76	1.76
Ab	98,90	99.00	99.60	99.40	99.50	99.50
An	0.70	0.20	0.10	0.20	0.20	0.20
Or	0.36	0.73	0.24	0.41	0.28	0.28

mineral. Late magmatic fluids destabilized the plagioclase and resulted in the formation of sericite where the alteration was incipient. The smaller grains in the matrix are strongly altered to kaolinite. The pyroxene altered to chlorite and generated opaque minerals. This late magmatic fluids rich in CO_2 used part of the Ca from plagioclase and/or pyroxene to form calcite. If it is considered that the original rocks are basalts and andesitic basalts, with original plagioclases of intermediate composition (50-70 An), the Ca needed to form calcite could have been derived from these plagioclases or from the associated pyroxenes. If all Ca was leached from the plagioclase the product probably would be a clay mineral or albite. It could be a reaction Ca-Na plag + H_2O + CO_2 albite + $CaCO_3$ + clay-mineral.

The heterogeneous alkali-feldspar of the UFA is the result of partial albitization of sanidine.

In some cases, the generated spherulitic textures in the UFA have probably resulted of an original volcanic glass devitrification. These spherulites of anorthoclasic and albitic compositions (EMP analyses) suggest that Na-rich late fluids affected and altered these textures.

The magmatic crystallization generated Ti - rich magnetite with exsolution lamellae of ilmenite, which upon interaction with a late fluid altered to TiO_2 (probably rutile) and hematite, according to the reaction: $4FeTiO_3 + O_2 \rightarrow 4TiO_2 + 2Fe_2O_3$. The interaction with this late fluid also promoted the migration of Ti into cleavage planes and the crystallization of ilmenite and rutile. Therefore, the process of autometasomatism occurred under high fugacity of oxygen. Illite observed in UFA units is an alteration product of sanidine, vitroclasts and/or shards and pumice.

The REE content variations from LMA to felsic rocks of UFA show clear parallelism between the spectrum of each group as well as within them, except for the strong negative Eu anomaly observed in UFA. In general, the progressive increase in total REE contents,

TABLE II

Analyses of oxides from tuffs, welded tuffs and flows of Upper Felsic Association – Acampamento Velho Alloformation. Mt = magnetite; Il = ilmenite; Ru = rutile. Scanning Electron Microscope data (SEM). n.d. = not detected. The detected presence of Si and Al is due to probable contamination of sanidine that is inside of the Ti-enriched magnetite.

Sample	SSB-32-1	SSB-32-1	MH-32-2	MH-35-1	MH-35-2	SSB-23a
rocks	tuff		welded tuff			flow
Mineral	Mt	Mt	Mt	Il	Ru	Mt
SiO_2	9.80	9.21	n.d.	17.58	4.12	0.99
TiO_2	N.d.	n.d.	7.45	35.81	89,83	15.44
Al_2O_3	1.61	1.12	0.47	11.63	2.04	n.d.
Fe_2O_3	87.94	89.10	92.08	33.35	1.73	83.57
MgO	n.d.	n.d.	n.d.	0.26	1.48	n.d.
K_2O	n.d.	n.d.	n.d.	1.36	0.80	n.d.
total1	100.00	99.99	100.00	99.99	100.00	100.00
Total	99.35	99.43	100.00	99.99	100.00	100.00
Cl	0.65	0.56	n.d.	n.d.	n.d.	n.d.
Si	4.85	0.13	n.d.	8.22	1.93	0.46
Al	0.85	0.11	0.25	6.16	1.08	n.d.
Ti	n.d.	n.d.	4.47	35.81	53.58	9.26
Fe_3	61.51	62.32	64.40	23.32	1.21	58.45
Mg	n.d.	n.d.	n.d.	0.16	n.d.	n.d.
K	n.d.	n.d.	n.d.	1.13	0.66	n.d.
Cations	67.21	62.56	69.12	74.80	58.73	68.17

from lesser to more evolved rocks (Almeida et al. 2002), shows no influence of the Na-rich fluid in the behavior of these elements.

For the LMA, the crystallization sequence is: (1) Ti-rich magnetite(?), (2) pyroxene, (3) plagioclase, (4) albite, resulting from the late introduction of Na- and CO_2-rich fluids, which affected mainly the plagioclase and pyroxene (subordinate), (5) sericite, chlorite and calcite from late solutions that altered the pyroxene, and sericite-kaolinite that altered the plagioclase.

For the UFA, the following order of crystallization was identified: (1) zircon, (2) Ti-rich magnetite, (3) sanidine, (4) quartz. The introduction of Na-rich late fluids affected the whole volcanic package with variable intensity, promoting the crystallization of (5) heterogeneous alkali-feldspar, (6) the de-estabilization of magnetite, (7) the formation of ilmenite and rutile and (8) partial albitization of spherulites. Finally, the alteration of sanidine, vitroclasts and/or shards and pumice to (9) illite took place.

ACKNOWLEDGMENTS

The authors wish to thank Fundação de Amparo à Pesquisa do Estado do Rio Grande do Sul (FAPERGS) for the financial support (project # 01/0881-5) and Universidade do Vale do Rio dos Sinos (UNISINOS) for the scholarship granted to Ricardo Medeiros. The reviewers are kindly acknowledged for their suggestions, which greatly helped to improve the manuscript.

RESUMO

Um estudo mineralógico de detalhe foi realizado nas rochas vulcânicas da Aloformação Acampamento Velho nos Cerros do Bugio, Perau e Serra de Santa Bárbara (Bacia do Camaquã), sudeste do Brasil. Este evento bimodal é constituído por duas associações: máfica inferior na base e félsica superior no topo. Foram estudados grãos de plagioclásio e feldspato alcalino com o uso de microssonda eletrônica, sendo que, magnetita, ilmenita, rutilo e ilita além de feldspato alcalino foram pesquisados através do microscópio eletrônico de varredura. Todas

Sample	MH21-21	MH37-32bb	MH37-35b	MH37-35c	MH37-38	MH37-44b	MH37-44c	MH37-47b	MH37-49	MH29-p2*	MH29-p2-2*	MH29-p2-2*	MH32-p1*	MH35-1*	MH35-2*
										heterogeneous alkaline feldspars					
Location	matrix	rim	rim	inter	core	rim	inter	rim	core	brigth	dark	brigth	matrix	In Mt	In Mt
SiO_2	93.40	84.78	88.03	86.09	95.48	85.10	90.06	97.38	89.14	59.73	68.16	52,01	45.12	67.70	55.12
TiO_2	n.d.	n.d.	n.d.	n.d.	n.d.	n.d.	n.d.	n.d.	n.d.	n.d.	n.d.	n.d.	n.d.	n.d.	0.58
Al_2O_3	3.64	8.92	7.66	7.45	0.18	9.32	6.02	1.16	6.74	14,48	16.30	28.17	23,46	18.57	27.23
Fe_2O_3	n.d.	n.d.	n.d.	n.d.	n.d.	n.d.	n.d.	n.d.	n.d.	n.d.	n.d.	n.d.	n.d.	3.75	4.31
FeO	0.07	0.12	0.23	0.74	0.15	0.39	0.714	0.05	0.12	n.d.	n.d.	n.d.	19.25	n.d.	n.d.
MgO	0.01	n.d.	0.01	n.d.	0.02	0.01	0.01	n.d.	n.d.	n.d.	n.d.	n.d.	n.d.	0.90	0.950
BaO	n.d.	0.10	0.02	0.03	n.d.	n.d.	0.01	n.d.	0.04	n.d.	n.d.	n.d.	n.d.	n.d.	n.d.
CaO	n.d.	0.06	0.02	0.08	0.01	0.12	0.14	0.01	0.09	n.d.	n.d.	n.d.	n.d.	n.d.	n.d.
Na_2O	0.15	3.84	1.49	1.05	0.35	1.78	1.57	0.11	1.17	7.38	6.85	7.29	n.d.	n.d.	n.d.
K_2O	2.21	2.41	3.80	4.13	1.49	4.96	3.34	0.34	3.25	18.41	8.69	11.65	12.18	9.07	11.82
Total	99.48	100.29	101.26	99.57	100.68	101.68	101.86	99.05	100.55	100.00	100.00	99.12	100.01	99.99	100.01
Si	15.82	14.66	15.00	14.94	15.91	14.64	15.23	16.30	15.19	27.92	31.86	24.31	21.09	31.65	25.76
Al	0.73	1.82	1.54	1.53	0.62	1.87	1.19	0.23	1.35	7.66	8.63	14.91	12.42	9.83	14.41
Fe_3	n.d.	n.d.	n.d.	n.d.	n.d.	n.d.	n.d.	n.d.	n.d.	n.d.	n.d.	n.d.	13.46	2.62	3.01
Ti	n.d.	n.d.	n.d.	n.d.	n.d.	n.d.	n.d.	n.d.	n.d.	n.d.	n.d.	n.d.	n.d.	n.d.	0.35
Fe_2	0.01	0.12	0.03	0.11	0.02	0.05	0.10	0.01	0.02	n.d.	n.d.	n.d.	n.d.	n.d.	n.d.
Mg	n.d.	n.d.	n.d.	n.d.	n.d.	n.d.	n.d.	0.01	n.d.	n.d.	n.d.	0.53	n.d.	0.55	0.57
Ba	n.d.	0.01	n.d.	0.01	n.d.	n.d.	n.d.	n.d.	n.d.	n.d.	n.d.	n.d.	n.d.	n.d.	n.d.
Ca	n.d.	0.01	n.d.	0.02	n.d.	0.02	0.03	0.01	0.02	n.d.	n.d.	n.d.	n.d.	n.d.	n.d.
Na	0.05	1.29	0.49	0.35	0.11	0.59	0.51	0.04	0.39	n.d.	5.58	n.d.	n.d.	n.d.	n.d.
K	0.48	0.53	0.82	0.92	0.32	1.08	0.72	0.07	0.71	15.28	n.d.	9.67	10.11	7.53	9.81
Cations	17.08	18.34	17.82	17.90	16.99	18.26	17.78	16.64	17.68	50.86	45.57	49.42	57.08	52.18	53.91
X	16.54	16.48	16.53	16.50	16.53	16.51	16.42	16.52	16.55	35.58	40.49	39.22	46.97	44.10	43.53
Z	0.54	1.85	1.36	1.39	0.46	1.75	1.36	n.d.	1.13	15.28	5.08	10.20	10.11	8.08	10.38
Ab	9.30	70.30	37.20	27.50	26,20	34.90	40.80	32.40	35.00	n.d.	100.00	n.d.	n.d.	n.d.	n.d.
An	n.d.	0.60	0.30	1.20	0.70	1.30	2.10	2.70	1.40	n.d.	n.d.	n.d.	n.d.	n.d.	n.d.
Or	90.70	29.06	62.50	71.28	73.15	63,82	57.09	64.86	63.60	100.00	n.d.	100.00	100.00	100.00	100.00

Fig. 5 – Table of analyses of sanidine and heterogeneous alkaline feldspar from welded tuffs of Upper felsic association – Acampamento Velho Alloformation. Data obtained through the electron microprobe (EMP) and scanning electron microscope (SEM*). inter = intermediary; In Mt = analyses realized in magnetite that is substituted by sanidine of matrix. n.d. = not detected.

as rochas foram afetadas por um processo de autometassomatismo sódico tardio. Nas rochas máficas, o plagioclásio cálcico foi transformado em albita e os piroxênios foram alterados. Nas rochas félsicas, a sanidina foi parcialmente pseudomorfoseada, transformando-se em feldspato alcalino heterogêneo. Nesta mesma associação, as magnetitas ricas em Ti se desestabilizam sendo parcialmente substituídas por ilmenita e rutilo. Para a associação máfica inferior, a seqüência de cristalização foi: (1) magnetita rica em titânio (?), (2) piroxênio e plagioclásio cálcico, (3) albita (alteração do plagioclásio cálcico), (4) sericita, clorita e calcita (alteração de piroxênio) e caolinita (alteração de plagioclásio/albita). Nas rochas da seqüência félsica superior: (1) zircão, (2) magnetita rica em Ti, (3) sanidina, (4) quartzo. A introdução de fluidos tardios ricos em Na promoveu a formação de (5) feldspato alcalino heterogêneo, (6) ilmenita e rutilo a partir de magnetita rica em Ti e (7) albita nas esferulitas. Por último, alteração da sanidina, vitroclastos e/ou shard e púmice em (8) ilita.

Palavras-chave: química mineral, metassomatismo sódico, aloformação Acampamento Velho, Orogenia Brasiliana.

REFERENCES

ALMEIDA DPM, ZERFASS H, BASEI MA, PETRY K AND GOMES CH. 2002. The Acampamento Velho Formation, a Lower Cambrian bimodal volcanic package: geochemical and stratigraphic studies from the Cerro do Bugio, Perau and Serra de Santa Bárbara (Caçapava do Sul, Rio Grande do Sul, RS – Brazil). Gondwana Res 5: 721–733.

ALMEIDA DPM, ZERFASS H, BASEI MA AND LOPES RC. 2003. Eventos vulcânicos alcalinos na Bacia do Camaquã: o vulcanismo Neoproterozoico III Acampamento Velho e o magmatismo Meso-Ordoviciano (?) Rodeio Velho. In: RONCHI LH AND ALTHOFF F (Eds), Caracterização e Modelamento de Depósitos Minerais. São Leopoldo: Universidade do Vale do Rio dos Sinos, p. 325–350.

ALMEIDA DPM, CONCEIÇÃO RV, CHEMALE JR F, KOESTER E, BORBA A AND PETRY K. 2005. Evolution of heterogeneous Mantle in the Acampamento Velho and Rodeio Velho volcanic events, Camaquã Basin, Southern Brazil. Gondwana Res 8: 479–492.

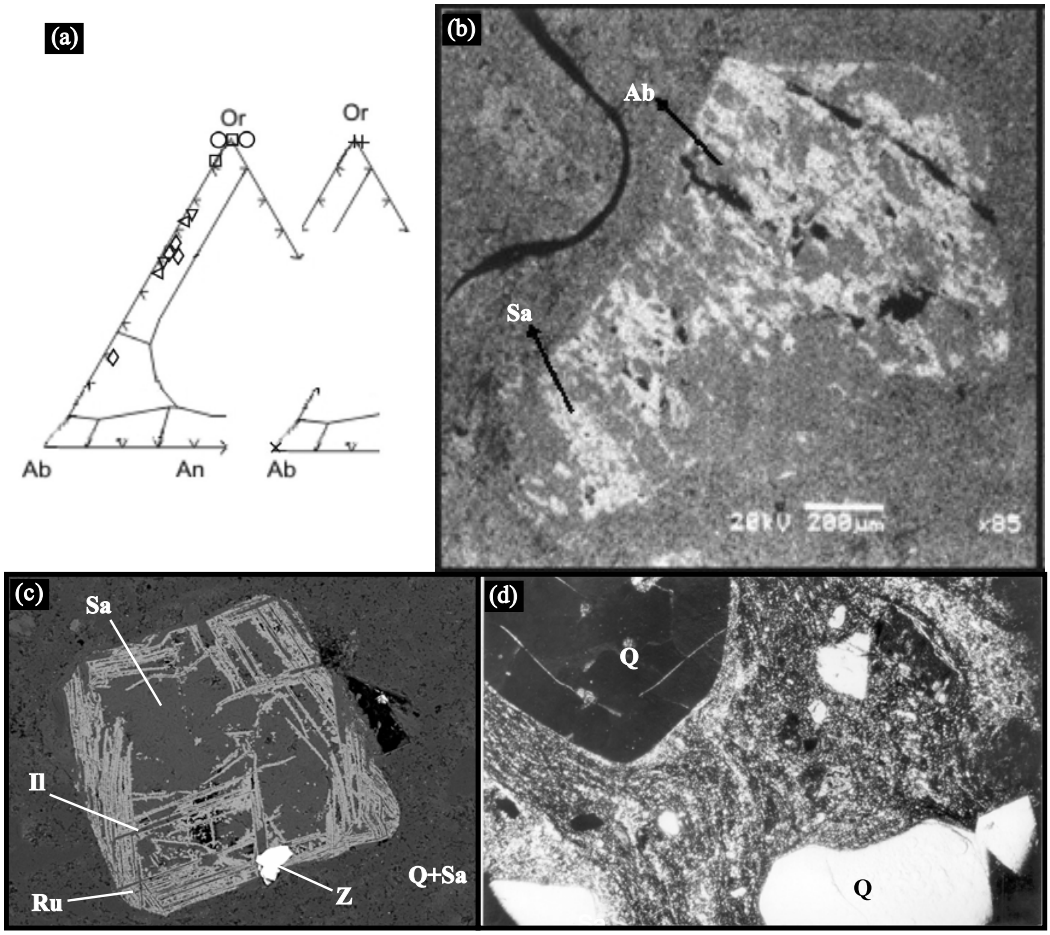

Fig. 6 – Welded tuff: (a) diagram Ab-Or-An (EMP and SEM), □ = matrix, ◊ = rim, Δ = inter, ∇ = core, + = brigth, x = dark, O = in Mt. (b) Photomicrography of crystalloclast of heterogeneous alkali- feldspar corroded by the matrix (analyzed through the EMP); (c) Photomicrography of Ti-rich magnetite crystalloclast is altered to ilmenita (IL), rutile (Ru) disposed according to twinning and/or cleavages with inclusions of zircon (Z) and replaced by sanidine (Sa) (SEM); (d) Photomicrography of crystalloclasts of quartz (Q), matrix of sanidine and quartz as stretched pseudomorphic shards and pumice (optical microscope PL).

BASEI MAS, SIGA JR O, MASQUELIN H, HARARA M, REIS NETO JM AND PRECIOZZI PF. 2000. The Dom Feliciano Belt of Brazil and Uruguay and its foreland domain, the Rio de la Plata Craton. In: CORDANI UG ET AL. (Eds), Tectonic Evolution of South America, p. 311–334.

CHEMALE JR F. 2000. Evolução geológica do Escudo Sul-rio-grandense. In: HOLZ M AND DE ROS LF (Eds), Geologia do Rio Grande do Sul. Centro de Investigação do Gondwana, Porto Alegre: Universidade Federal do Rio Grande do Sul, p. 13–52.

CORDANI UG, HALPERN M AND BERENHOLC M. 1974. Comentários sobre as determinações da Folha de Porto Alegre. In: DNPM, CARTA GEOLÓGICA DO BRASIL AO MILIONÉSIMO, texto explicativo da Folha de Porto Alegre e Lagoa Mirim, p. 70–84.

CULLERS RL AND GRAF JL. 1984. Rare earth elements in igneous rocks of the continental crust: predominantly basic and ultrabasic rocks. In: ANDERSON P (Ed), Rare earth Element Geochemistry, Amsterdam: Elsevier 2: 237–274.

FERNANDES LAD, TOMMASI A AND PORCHER CC. 1992. Deformation patterns in the southern Brazilian branch of the Dom Feliciano belt: a reappraisal. J S Amer Earth Sci 5: 71–96.

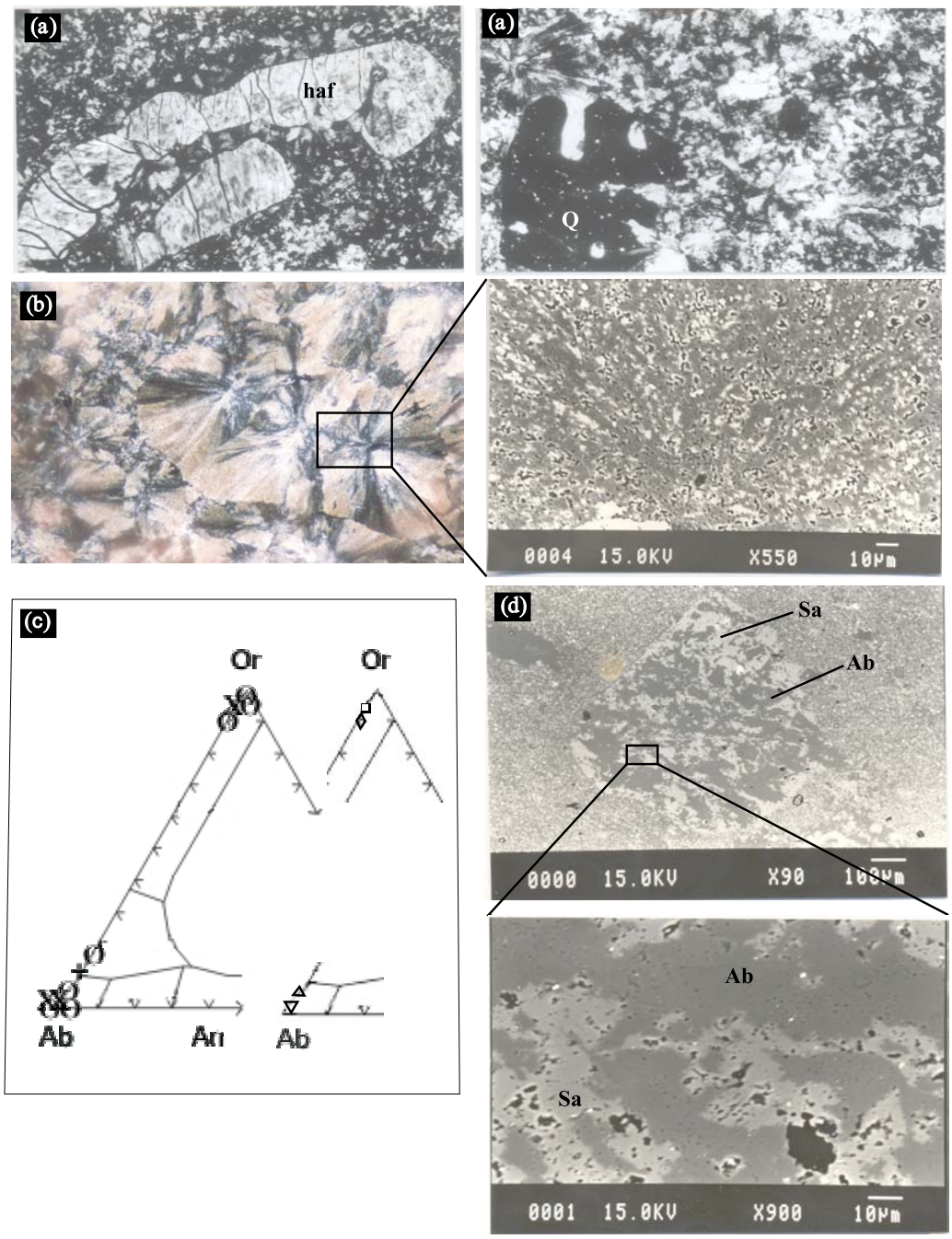

Fig. 7 – Rhyolite flows: (a) Photomicrography of heterogeneous alkali-feldspar (haf) and quartz (Q) phenocrysts with gulfs of corrosion and conchoidal fractures (optical microscope PL, 40 x); (b) Photomicrography of spherulites (optical microscope PPL) with fine aggregates of anorthoclase and albite grains as well as Fe oxides (EMP); (c) diagram Ab-Or-An (EMP), O = core, x = rim, + = matrix, ◊ = bright core, ∇ = dark core, □ = bright rim, Δ = dark rim; (d) Photomicrography of heterogeneous alkali-feldspar phenocryst and its detailed view (EMP).

Sample	123a2a	123a2b	123a2c	123a2d	333b1a	333b1b	33b2a	333b2b	69.2-1a	69.2-1b	69.2-2a	69.2-2b	ps60-1a	ps60-3
Location	bright core	dark core	bright rim	dark rim	core	rim	core	core	core	rim	core	rim	core	matrix
	heterogeneous alkaline feldpars				sanidine		albita		albita		albita		sanidine	albita
SiO_2	64.12	67.78	64.57	67.78	64.08	64.08	86.11	84.45	68.65	68.57	67.99	68.29	64.51	67.56
Al_2O_3	18.31	19.72	18.47	19.10	18.26	18.43	8.36	9.56	19.54	19.77	19.52	19.35	18.40	19.45
FeO	n.d.	n.d.	n.d.	n.d.	n.d.	n.d.	n.d.	0.67	n.d.	n.d.	n.d.	n.d.	n.d.	0.67
Na_2O	0.35	11.71	0.28	11.21	0.45	0.25	4.33	4.68	11.6 0	12.10	11.77	11.64	n.d.	11.24
K_2O	16.36	0.18	16.6	1.11	16.32	16.73	0.43	1.39	n.d.	n.d.	n.d.	0.08	19.72	1.48
Total	99.14	99.39	99.92	99.20	99.11	99.49	99.23	100.43	99.79	100.35	99.28	99.36	99.63	100.37
Si	2.99	2.98	2.99	3.00	2.99	2.99	4.50	4.41	3.00	2.99	2.99	3.00	3.00	2.97
Al	1.01	1.02	1.01	1.00	1.01	1.01	0.52	0.59	1.01	1.02	1.01	1.00	1.01	1.01
Fe_2	n.d.	n.d.	n.d.	n.d.	n.d.	n.d.	n.d.	0.02	n.d.	n.d.	n.d.	n.d.	n.d.	0.02
Na	0.03	1.00	0.03	0.98	0.04	0.02	0.44	0.47	0.98	1.01	1.00	0.99	n.d.	0.96
K	0.97	0.01	0.98	0.06	0.97	1.00	0.03	0.09	n.d.	n.d.	n.d.	n.d.	0.99	0.08
Cations	5.00	50.10	5.01	5.04	5.01	5.02	5.49	5.58	4.99	5.02	5.00	4.99	5.00	5.04
X	4.00	4.00	4.00	4.00	4.00	4.00	5.02	5.00	4.01	4.01	4.00	4.00	4.01	3.98
Z	1.00	1.01	1.01	1.04	1.01	1.02	0.47	0.58	0.98	1.01	1.00	0.99	0.99	1.06
Ab	3.00	99.00	3.00	94.20	4.00	2.00	93.60	83.90	100.00	100.00	100	100	n.d.	92.30
An	n.d.	n.d.	n.d.	n.d.	n.d.	n.d.	n.d.	n.d.	n.d.	n.d.	n.d.	n.d.	n.d.	n.d.
Or	97.00	0.99	97.03	5.77	96.04	98.04	6.38	16.07	n.d.	n.d.	n.d.	n.d.	100.00	7.69

Fig. 8 – Table of analyses of sanidine (electron microprobe), albite and heterogeneous alkaline feldspar from rhyolitic lavas of Upper Felsic Association – Acampamento Velho Alloformation. n.d. = not detected.

FRAGOSO-CESAR ARS, CESAR ARSF, FAMBRINI G, PAES-DE-ALMEIDA R, PELOSI A, JANIKIAN L, RICCOMINI C, NOGUEIRA A AND SAES G. 2000. The Camaquã Extensional Basin: Neoproterozoic-Early Paleozoic Transition in the State of Rio Grande do Sul, Brazil. Rev Bras Geoc 30: 438–441.

GRESSE PG, CHEMALE JR F, SILVA LC, WALRAVEN F AND HARTMANN LA. 1996. Late to post orogenic basins of the Pan-African-Brasiliano collision orogen in Southern Africa and Southern Brazil. Basin Res 8: 157–171.

PAIM PSG, CHEMALE JR F AND LOPES RC. 2000. A Bacia do Camaquã. In: HOLZ M AND DE ROS LF (Eds), Geologia do Rio Grande do Sul, Porto Alegre: Universidade Federal do Rio Grande do Sul, p. 231–274.

SOMMER CA, LIMA EF AND NARDI LVS. 1999. O vulcanismo alcalino do Platô do Taquarembó, Dom Pedrito, RS. Rev Bras Geoc 29: 245–254.

SOMMER CA, LIMA EF, NARDI LVS, FIGUEIREDO AMG AND PIEROSAN R. 2005. Potassic and low- and high-Ti mildly alkaline volcanism in the Neoproterozoic Ramada Plateau, southermost Brazil. J S Amer Earth Sci 18: 237–254.

TAYLOR SR AND MACLENNAN SM. 1985. The continental crust: its composition and evolution. Blackwell Scientific Publication Oxford, 312 p.

TEIXEIRA W. 1982. Folhas SH.22 – Porto Alegre, SI.22 – Lagoa Mirim e SH.21 – Uruguaiana: interpretação dos dados radiométricos e evolução geocronológica. Projeto RADAMBRASIL, Florianópolis, SC, Brasil.

WILDNER W, NARDI LVS AND LIMA EF. 1999. Post-Collisional Alkaline Magmatism on the Taquarembó Plateau: A Well Preserved Neoproterozoic-Cambrian Plutono-Volcanic Association in Southern Brazil. Intern Geol Review 41: 1082–1098.

ZERFASS H AND ALMEIDA DPM. 1997. Mapa Geológico da região dos Cerros Bugio e Perau, Município de Caçapava do Sul, RS. Acta Geol. Leopoldensia, Série Mapas XX(3): 1–15.

ZERFASS H, ALMEIDA DPM AND GOMES CH. 2000. Faciology of the Acampamento Velho Formation volcanic rocks (Camaquã Basin) in the region of Serra de Santa Bárbara, Cerro do Perau and Cerro do Bugio (Municipality of Caçapava do Sul – RS). Rev Bras Geoc 30: 375–379.